

Anomalous Temperature Dependence of High-Harmonic Generation in Mott InsulatorsYuta Murakami^{1,2}, Kento Uchida,³ Akihisa Koga¹, Koichiro Tanaka,^{3,4} and Philipp Werner⁵¹*Department of Physics, Tokyo Institute of Technology, Meguro, Tokyo 152-8551, Japan*²*Center for Emergent Matter Science, RIKEN, Wako, Saitama 351-0198, Japan*³*Department of Physics, Graduate School of Science, Kyoto University, Sakyo-ku, Kyoto 606-8502, Japan*⁴*Institute for Integrated Cell-Material Sciences, Kyoto University, Sakyo-ku, Kyoto 606-8501, Japan*⁵*Department of Physics, University of Fribourg, 1700 Fribourg, Switzerland*

(Received 14 April 2022; accepted 12 September 2022; published 3 October 2022)

We reveal the crucial effect of strong spin-charge coupling on high-harmonic generation (HHG) in Mott insulators. In a system with antiferromagnetic correlations, the HHG signal is drastically enhanced with decreasing temperature, even though the gap increases and the production of charge carriers is suppressed. This anomalous behavior, which has also been observed in recent HHG experiments on Ca_2RuO_4 , originates from a cooperative effect between the spin-charge coupling and the thermal ensemble, as well as the strongly temperature-dependent coherence between charge carriers. We argue that the peculiar temperature dependence of HHG is a generic feature of Mott insulators, which can be controlled via the Coulomb interaction and dimensionality of the system. Our results demonstrate that correlations between different degrees of freedom, which are a characteristic feature of strongly correlated solids, have significant and nontrivial effects on nonlinear optical responses.

DOI: [10.1103/PhysRevLett.129.157401](https://doi.org/10.1103/PhysRevLett.129.157401)

High-harmonic generation (HHG) is a fundamental nonlinear optical phenomenon with potentially important technological applications. It was first reported in atomic gases [1] and is utilized in attosecond laser sources as well as spectroscopies [2]. The recent observation of HHG in solids, in particular semiconductors and semi-metals [3–17], extends the scope of HHG studies. HHG in semiconductors and semimetals can be well described by the dynamics of independent electrons (independent-particle picture) [18–34], which enables the HHG spectroscopy of band information such as dispersion relations [5,35–38]. On the other hand, the effects of electronic correlations are often taken into account phenomenologically and a detailed understanding of their role in solid-state HHG is lacking [39–42]. This understanding is, however, essential for the exploration of HHG and the application of HHG spectroscopy in correlated materials.

The new research frontier of HHG in strongly correlated systems (SCSs) has attracted considerable interest both on the theoretical [43–55] and experimental [56–58] sides. In contrast to semiconductors, which can be described in terms of electrons and holes, the driven state of SCSs involves various types of many-body elemental excitations. This makes the mechanism and features of HHG in SCSs nontrivial. Previous studies revealed the direct connection between many-body excitations and HHG in SCSs [44,48,51], suggesting possible spectroscopic applications of HHG to detect many-body states [51] as well as photoinduced phase transitions [43]. On the other hand, very recently, an unexpected exponential enhancement of

the HHG signal with increasing gap size has been reported in the Mott insulator Ca_2RuO_4 [56], see Fig. 1(a). Since a larger gap should suppress the excitation of charge carriers, this increase is opposite of the behavior expected in semiconductor HHG. Such a counterintuitive result calls for a deeper theoretical understanding of HHG in SCSs. A hallmark of SCSs is the coupling between different degrees of freedom, such as charges, orbitals, and spins. These correlations are at the origin of rich physical properties observed in equilibrium SCSs [59,60]. However, their role in highly nonlinear optical phenomena such as HHG is hardly known.

In this Letter, we reveal the crucial role of spin-charge coupling on HHG in Mott insulators analyzing the Hubbard model. Previous works showed that HHG in Mott insulators originates from the coherent dynamics of a pair of local many-body states—a doublon (doubly occupied state) and holon (empty state)—generated by strong fields, where the three-step model picture is applicable [44,51]. The kinematics of doublons and holons is strongly correlated with spins, since their hopping disturbs the spin background. We demonstrate that this spin-charge coupling and its cooperation with thermal fluctuations produces a drastic enhancement of the HHG intensity, accompanied with an increasing Mott gap, as observed in Ca_2RuO_4 [Fig. 1(b)]. These results demonstrate that strong correlations between active degrees of freedom in SCSs can result in counterintuitive behaviors of highly nonlinear optical phenomena such as HHG.

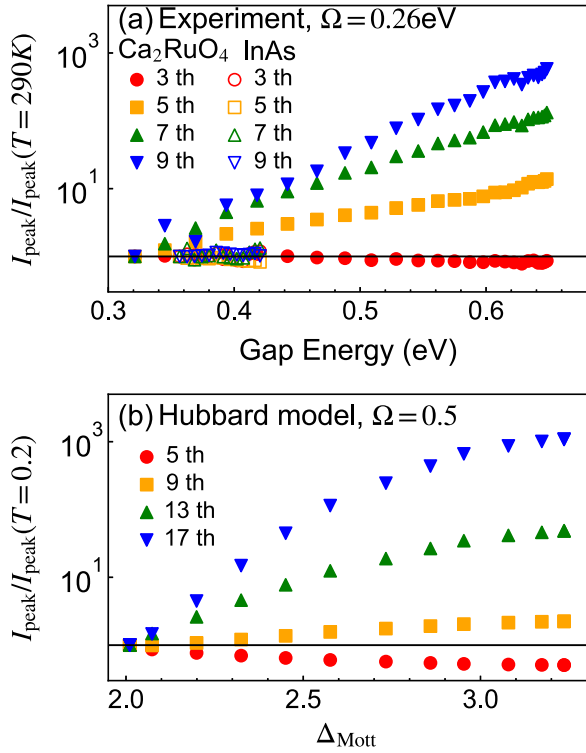


FIG. 1. (a) Experimental HHG intensity at the indicated HHG peaks as a function of the optical gap for Ca_2RuO_4 (Mott insulator) and InAs (semiconductor), reproduced from Ref. [56]. The temperature T is modified in the range $T \in [290, 50]$ K. (b) DMFT results for the intensity at the indicated HHG peaks as a function of the Mott gap (Δ_{Mott}) for the single-band Hubbard model in the Mott insulating phase.

We focus on the single-band Hubbard model, which is a standard model for SCSs. The Hamiltonian is

$$\hat{H}(t) = -t_{\text{hop}} \sum_{\langle ij \rangle} e^{i\phi_{ij}(t)} \hat{c}_{i\sigma}^\dagger \hat{c}_{j\sigma} + U \sum_i \hat{n}_{i\uparrow} \hat{n}_{i\downarrow}, \quad (1)$$

where $\hat{c}_{i\sigma}^\dagger$ is the creation operator for an electron with spin σ at site i , $\langle ij \rangle$ indicates a pair of neighboring sites, and $\hat{n}_{i\sigma} = \hat{c}_{i\sigma}^\dagger \hat{c}_{i\sigma}$. t_{hop} is the hopping parameter and U is the on-site interaction. The electric field is included via a Peierls phase ϕ_{ij} , see Supplemental Material [61]. We mainly use the nonequilibrium dynamical mean-field theory (DMFT) [63–67] to solve this problem and focus on the Bethe lattice for simplicity [68]. The qualitatively same results are obtained for the two-dimensional square lattice, see Ref. [61]. In the following, we use a quarter of the bandwidth at $U = 0$ as the energy unit and mainly consider $U = 6$. If our energy unit corresponds to 0.5 eV, the Mott gap ($\Delta_{\text{Mott}} \simeq 3$, see below) corresponds to 1.5 eV. This is a typical gap size for cuprates, which are often described by the Hubbard model.

We consider the half filled system, which becomes a Mott insulator for large enough U in equilibrium. While the Mott insulator can be realized in the paramagnetic (PM)

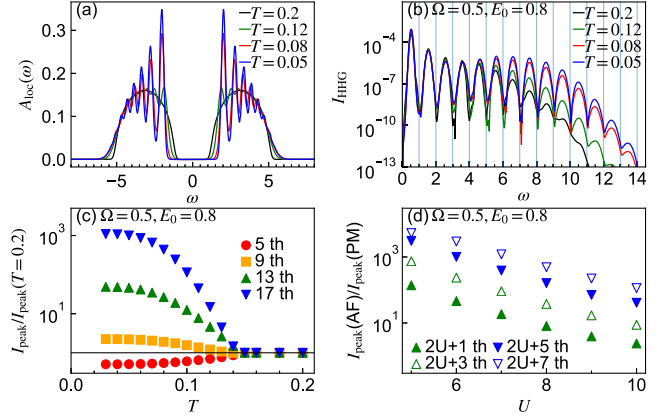


FIG. 2. (a) Local spectral functions $A_{\text{loc}}(\omega)$ in equilibrium. (b) HHG spectra of the Mott insulator computed with DMFT for various T . (c) The intensity at the peaks of the HHG spectra as a function of T . The peak intensity is normalized by the value at $T = 0.2$ (PM phase). For (a)–(c), we use $U = 6$. (d) U dependence of the increase ratio of the HHG peaks. In order to take into account the change of the Mott gap, we compare the $(2U + n)$ th HHG peaks. We use $T = 0.2$ for the PM phase, while we use $T = 0.3/U$ for the AF state to take account of the change of $J_{\text{ex}} \propto (1/U)$. The excitation parameters are $E_0 = 0.8$, $\Omega = 0.5$, $t_0 = 75$, and $\sigma = 15$.

phase, the system on the bipartite lattice exhibits an antiferromagnetic (AF) phase below the Néel temperature T_c ($\simeq 0.15$). The corresponding evolution of the single-particle spectra is shown in Fig. 2(a). With decreasing temperature T , the Mott gap Δ_{Mott} increases. In the PM phase, the upper and lower Hubbard bands are featureless. On the other hand, in the AF phase, peak structures develop within the bands, indicating the formation of spin polarons [60,69,70]. When an electron is added to (removed from) the system, a doublon (holon) is created; see Supplemental Material [61] for schematics. When this doublon (holon) moves around, it can disturb the spin background at the cost of multiples of the exchange energy $J_{\text{ex}} (= 4t_{\text{hop}}^2/U)$. This results in strong spin-charge coupling, of which the spin polaron is one manifestation.

Now we discuss the kinematics of doublons and holons accompanied by a disturbance of the spin configurations and its effect on highly nonlinear optical phenomena. We study the T dependence of HHG in Mott insulators excited with frequency Ω smaller than the Mott gap Δ_{Mott} . We mainly use $\Omega = 0.5$ in the following. If our energy unit corresponds to 0.5 eV, this is a midinfrared excitation with 0.25 eV, whose period T_p is about 16 fs. From the T dependence of the single particle spectra, one would naively speculate that the HHG intensity is suppressed by lowering temperature, since the enhancement of the gap reduces the tunneling probability (see Ref. [61]) and the formation of the spin polarons suggests a reduced mobility of the charge carriers. However, the T dependence turns out to be the *opposite* of this naive expectation.

Applying a Gaussian electric field pulse $E(t)$, we evaluate the HHG intensity $I_{\text{HHG}}(\omega)$ from the Fourier transformation of the current $J(t)$ as $I_{\text{HHG}}(\omega) = |\omega J(\omega)|^2$. The pulse is characterized by the standard deviation σ , the center t_0 , and the maximum field strength E_0 . We show the resulting HHG spectra for various temperatures in Fig. 2(b) and plot the T dependence of the relative intensity of the HHG peaks in Fig. 2(c). $I_{\text{HHG}}(\omega)$ is strongly enhanced above Δ_{Mott} and the width of the HHG plateau is enhanced with decreasing temperature. The increase in the ratio of HHG signals is larger for the higher harmonic peaks. Above T_c , the T dependence becomes very weak. As a function of the gap, the intensity increases almost exponentially, as illustrated in Fig. 1(b). Importantly, the DMFT results of the simple Hubbard model reproduce the qualitative features of the HHG spectrum and the empirical scaling law observed in Ca_2RuO_4 [56] [see Fig. 1(a) and [61]].

To reveal the origin of this T dependence, we consider the U dependence of the relative increase of the HHG signal [Fig. 2(d)]. For large U , the bandwidth of the upper and lower Hubbard bands is insensitive to U and the Mott gap scales almost linearly with U . Therefore, in order to focus on the contribution from the kinetic energy of the doublon-holon pair, we compare $I_{\text{HHG}}(\omega)$ for the same $\omega - U$. It turns out that the increase ratio monotonically decreases with increasing U . Since J_{ex} is reduced with increasing U , the disturbance of the spin background costs less energy, and the spin-charge coupling becomes weaker. Hence, the U dependence of the HHG increase ratio suggests that the anomalous T dependence of HHG is related to the spin-charge coupling.

Next we perform a subcycle analysis considering a windowed Fourier transform $J(\omega, t_p) = \int dt e^{i\omega t} F_{\text{window}}(t - t_p) J(t)$ and evaluating $I_{\text{HHG}}(\omega, t_p) \equiv |\omega J(\omega, t_p)|^2$. $I_{\text{HHG}}(\omega, t_p)$ provides the time-resolved spectral features of the emitted light around t_p . Since HHG in Mott insulators mainly originates from the recombination of doublon-holon pairs [44,51], the subcycle spectra reveal the recombination time of the pairs and their energy at that time. In Figs. 3(a) and 3(b), we show $I_{\text{HHG}}(\omega, t_p)$ in the PM and AF phases. In both cases, the dominant intensity appears at early times within one period, suggesting that only short trajectories of the doublon-holon pairs contribute to the HHG signal. In other words, the coherence time of the doublon-holon pair is very short ($< T_p/4$) compared to one cycle of the pulse field and to the coherence times typically considered in the analysis of semiconductors; see, e.g., Fig. 6 in Ref. [20]. The kinematics estimated from the peak position of $I_{\text{HHG}}(\omega, t_p)$ at each ω as a function of t_p is represented with red dashed (blue dot-dashed) lines for the AF (PM) phase in Figs. 3(a) and 3(b). These lines define the function $f_\omega(t_p)$. The difference between the blue and red lines is mostly explained by the difference in the gap size ($\simeq 1.1$), indicating that the trajectory of the doublon-holon

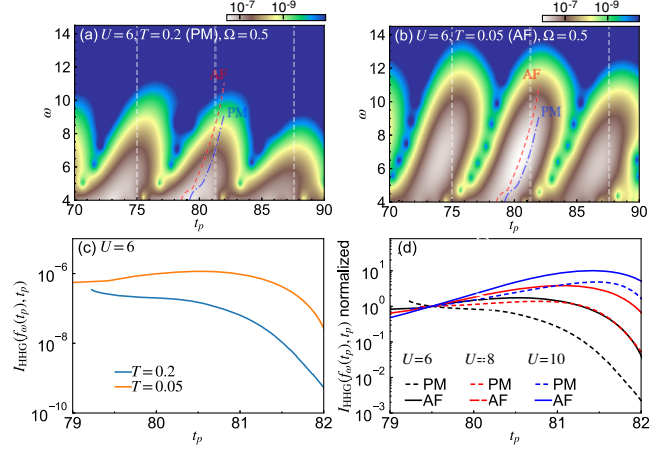


FIG. 3. (a) and (b) Subcycle spectra $I_{\text{HHG}}(\omega, t_p)$ for $U = 6$ at (a) $T = 0.2$ (PM phase) and at (b) $T = 0.05$ (AF phase). A Gaussian window with standard deviation $\sigma' = 0.9$ is used. The red dashed (blue dot-dashed) lines indicate the maxima of $I_{\text{HHG}}(\omega, t_p)$ at $T = 0.05$ ($T = 0.2$) at a given ω as a function of t_p around $t_p = 80$, which defines the function $f_\omega(t_p)$. The vertical dashed lines indicate the times when the electric field $E(t) = 0$. (c) Intensity $I_{\text{HHG}}(\omega, t_p)$ along the lines $f_\omega(t_p)$ for $U = 6$. (d) Normalized intensity $I_{\text{HHG}}(\omega, t_p)$ along the lines $f_\omega(t_p)$ for the indicated values of U . We use $T = 0.2$ for the PM phase and $T = 0.3/U$ for the AF states to take account of the change of $J_{\text{ex}} \propto (1/U)$. $I_{\text{HHG}}(f_\omega(t_p), t_p)$ is renormalized by the value at $t_p = 79.5$ in each case. The excitation parameters are the same as in Fig. 2.

pair is almost the same in the AF and PM phases. The main difference is the coherence time of the pair.

To quantify this, we show in Fig. 3(c) the intensity along the peaks, $I_{\text{HHG}}(f_\omega(t_p), t_p)$. The results indeed show that for the higher T the intensity decays faster, suggesting that the dephasing time of the doublon-holon pair is shorter. This is in stark contrast to the behavior of the charge distribution, where the absence of the AF spin background at high T leads to a slower relaxation [71–73]. On the other hand, with increasing U , the behavior of $I_{\text{HHG}}(f_\omega(t_p), t_p)$ in the AF and PM phases becomes more similar, see Fig. 3(d). Furthermore, the peak in $I_{\text{HHG}}(f_\omega(t_p), t_p)$ becomes clearer, which indicates that the intensity coming from longer-time trajectories of the doublon-holon pairs and hence the coherence time are increased. This feature appears counterintuitive, because the single-particle spectrum becomes highly incoherent for large U [60,70] and demonstrates that HHG in SCSs is not directly related to the single-particle spectra, in contrast to semiconductors [44,48,51].

These behaviors can be consistently explained in terms of the spin-charge coupling. To directly compare cases with and without spin-charge coupling, we switch to the one-dimensional (1D) Hubbard model with a staggered magnetic field B_{stagg}^z . In one dimension, without B_{stagg}^z , the kinematics of the doublons and holons is independent of

the spin degrees of freedom (spin-charge separation), while for $B_{\text{stagg}}^z \neq 0$, the hopping of a doublon (holon) creates a mismatch between the staggered field and the spin configuration, as it happens in higher-dimensional systems without field, see Supplemental Material [61] for schematics. With this setup, the 1D model can mimic the spin-charge coupling in higher dimensions. The infinite time-evolving block decimation (ITEBD) [74] allows one to compute accurate results for this model at $T = 0$ in the thermodynamic limit.

We show the HHG spectra for various B_{stagg}^z in Fig. 4(a) and the corresponding subcycle analysis in Figs. 4(b) and 4(c). For small B_{stagg}^z , the expected HHG peaks at $(2n + 1)\Omega$ in $I_{\text{HHG}}(\omega)$ are not clear, suggesting that the system is not fully time periodic during the pulse. This is attributed to the long coherence time of the doublon-holon pair, which leads to the interference of many quasiclassical trajectories within the three-step model [20]. Indeed, the subcycle spectra for small B_{stagg}^z suggest that long trajectories of doublon-holon pairs strongly contribute to the HHG signal, see Fig. 4(b) [51]. With increasing B_{stagg}^z , the HHG intensity becomes weaker but the HHG peaks become clearer at $(2n + 1)\Omega$. Here, B_{stagg}^z is chosen to be comparable to J_{ex} . In the subcycle spectrum, the weight is shifted to earlier times in one period, see Fig. 4(c), as it is the case in the DMFT results in Fig. 3(b) at low T . These results show that the coherence time of the doublon-holon pair is efficiently suppressed by the spin-charge coupling, which consistently

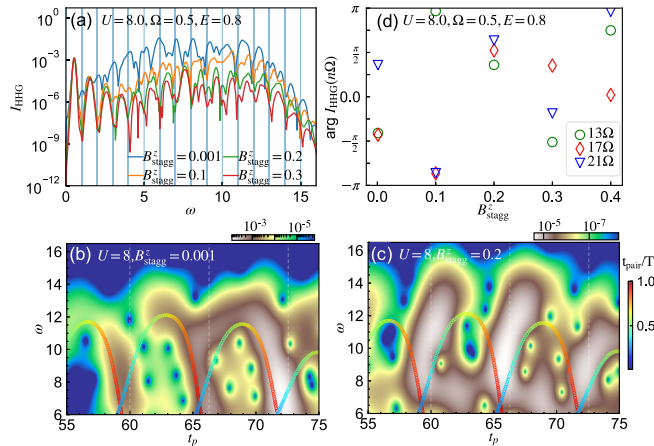


FIG. 4. (a) I_{HHG} for different B_{stagg}^z and subcycle analysis for (b) $B_{\text{stagg}}^z = 0.001$ and (c) $B_{\text{stagg}}^z = 0.2$. A Gaussian window with $\sigma' = 0.9$ is used. The colored markers indicate the energy emitted at t_p by the recombination of a doublon-holon pair, which is predicted from the three-step model using the doublon and holon dispersions from the Bethe ansatz [51]. The color indicates the time interval between the recombination and the creation of the doublon-holon pair t_{pair} , and $T_p = (2\pi/\Omega)$. (d) Phase of the Fourier component of $J(\omega)$ at $\omega = n\Omega$ (n is an integer). In all panels, we set $U = 8$, and the excitation parameters are $\Omega = 0.5$, $E_0 = 0.8$, $t_0 = 60$, and $\sigma = 15$.

explains the behavior of the DMFT results at low temperatures. The short coherence time reduces the interference between different quasiclassical trajectories and results in clear HHG peaks both in the DMFT data and the ITEBD data for nonzero B_{stagg}^z .

The reduction of the coherence time of the doublon-holon pair with increasing T can be understood as a cooperative effect of the spin-charge coupling and the thermal ensemble. At nonzero temperatures, the initial equilibrium state is described by an ensemble of eigenstates, represented by the density matrix $\hat{\rho} \propto e^{-\beta\hat{H}}$. In such a system, the total current induced by the field can be calculated as the ensemble average over the individual currents evaluated for these eigenstates. With increasing T , the weight of the high-energy states increases. In our case, at higher temperatures, spin configurations different from the AF ground state are activated, see Ref. [61]. The dynamics of the doublon or holon is different for each configuration, since the energy transfer to the spin background during an excursion depends on the spin configuration. This should produce emitted light with different phases for different spin configurations, resulting in phase cancellations after the ensemble average, and thus reduce the coherence between the doublon-holon pairs with increasing T . Note that this effect does not rely on long-range magnetic ordering and is also relevant in the PM phase, but is absent without spin-charge coupling. Namely, for small J_{ex} , weaker cancellations between different spin configurations are expected, which explains the results in Fig. 3(d) and the reduction of the enhancement of the HHG signal with larger U in Fig. 2(d). To exemplify that the spin-charge coupling can indeed provide such phase shifts, in Fig. 4(d), we show the B_{stagg}^z dependence of the phase of $J(\omega)$ for $\omega = n\Omega$ (with n some integer). The result suggests that the phase is sensitive to B_{stagg}^z , which supports the above argument. Hence, the modification of the coherence time due to the spin-charge coupling and thermal fluctuations dominates over the reduction of the tunneling rate by the gap opening, leading to an enhancement of I_{HHG} at lower temperatures.

The strong T dependence of the HHG spectrum observed in Mott insulators is not expected in typical semiconductors. In the theoretical analysis of HHG in semiconductors, a short dephasing time T_2 of a few femtoseconds for an electron-hole pair is often used. The main origin of the fast dephasing is the experimental setup, i.e., the dephasing by the propagation of light and the inhomogeneity of the field strength [30,75], which is insensitive to temperature. Another relevant factor is the electron-electron scattering among excited carriers in semiconductors [76,77]. Still, this is also expected to be insensitive to temperature, since thermal fluctuations cannot efficiently excite carriers across the gap. These considerations are supported by the experimental HHG spectrum for the semiconductor InAs shown in Fig. 1(a).

In summary, our theoretical study revealed important effects of strong spin-charge coupling on the coherent carrier dynamics in Mott insulators, which leads to the counterintuitive enhancement of HHG accompanied by a gap enhancement. Spin-charge coupling is inevitable in Mott insulators in dimensions larger than 1, so that this peculiar behavior should be a generic feature of HHG in SCSs (see Supplemental Material [61]). In addition, in multiorbital systems like Ca_2RuO_4 , the orbital-charge coupling should have a similar effect as the spin-charge coupling (see Ref. [61]) [78]. These insights demonstrate the important role of correlations in highly nonlinear optical responses and provide useful guidance for the future exploration of HHG in SCSs. On the one hand, our results suggest that the T dependence of I_{HHG} can be controlled by changing the ratio U/t_{hop} , which is feasible with the application of chemical or physical pressure. On the other hand, to realize a strong HHG signal, 1D Mott systems are more favorable than higher-dimensional ones due to the absence of spin-charge coupling. The recovery of coherence and the possible increase of the HHG intensity due to the reduction of the dimensionality could be systematically analyzed by exploiting the dimensional crossover in ladder-type compounds such as $\text{Sr}_{n-1}\text{Cu}_{n+1}\text{O}_{2n}$ [59]. Furthermore, the sensitivity of HHG to the temperature and spin-charge coupling suggests possible HHG-based techniques for detecting and characterizing thermal and nonthermal phases and for measuring the strength of the spin-charge coupling. In the future, it will also be interesting to study HHG with more sophisticated methods, such as cluster DMFT, to reveal the role of spin fluctuations.

The calculations have been performed on the Beo05 cluster at the University of Fribourg. This work is supported by Grant-in-Aid for Scientific Research from JSPS, KAKENHI Grants No. JP20K14412 (Y.M.), No. JP19K14632, No. JP22K03484, No. JP22K18322 (K.U.) No. JP21H05017 (Y.M., K.U., K.T.), No. JP19H05821, No. JP18K04678, No. JP17K05536 (A.K.), JST CREST Grant No. JPMJCR1901 (Y.M.), and ERC Consolidator Grant No. 724103 (P.W.). The nonequilibrium DMFT calculations have been implemented using the open source library NESSI [67].

[1] M. Ferray, A. L'Huillier, X.F. Li, L.A. Lompre, G. Mainfray, and C. Manus, *J. Phys. B* **21**, L31 (1988).
 [2] F. Krausz and M. Ivanov, *Rev. Mod. Phys.* **81**, 163 (2009).
 [3] S. Ghimire, A. D. DiChiara, E. Sistrunk, P. Agostini, L. F. DiMauro, and D. A. Reis, *Nat. Phys.* **7**, 138 (2011).
 [4] O. Schubert, M. Hohenleutner, F. Langer, B. Urbanek, C. Lange, U. Huttner, D. Golde, T. Meier, M. Kira, S. W. Koch, and R. Huber, *Nat. Photonics* **8**, 119 (2014).

[5] T. T. Luu, M. Garg, S. Y. Kruchinin, A. Moulet, M. T. Hassan, and E. Goulielmakis, *Nature (London)* **521**, 498 (2015).
 [6] G. Vampa, T. J. Hammond, N. Thire, B. E. Schmidt, F. Legare, C. R. McDonald, T. Brabec, and P. B. Corkum, *Nature (London)* **522**, 462 (2015).
 [7] F. Langer, M. Hohenleutner, C. P. Schmid, C. Pöllmann, P. Nagler, T. Korn, C. Schüller, M. Sherwin, U. Huttner, J. Steiner, S. Koch, M. Kira, and R. Huber, *Nature (London)* **533**, 225 (2016).
 [8] M. Hohenleutner, F. Langer, O. Schubert, M. Knorr, U. Huttner, S. Koch, M. Kira, and R. Huber, *Nature (London)* **523**, 572 (2015).
 [9] G. Ndashimiye, S. Ghimire, M. Wu, D. A. Browne, K. J. Schafer, M. B. Gaarde, and D. A. Reis, *Nature (London)* **534**, 520 (2016).
 [10] H. Liu, Y. Li, Y. S. You, S. Ghimire, T. F. Heinz, and D. A. Reis, *Nat. Phys.* **13**, 262 (2017).
 [11] Y. S. You, D. A. Reis, and S. Ghimire, *Nat. Phys.* **13**, 345 (2017).
 [12] N. Yoshikawa, T. Tamaya, and K. Tanaka, *Science* **356**, 736 (2017).
 [13] H. A. Hafez, S. Kovalev, J.-C. Deinert, Z. Mics, B. Green, N. Awari, M. Chen, S. Germanskiy, U. Lehnert, J. Teichert, Z. Wang, K.-J. Tielrooij, Z. Liu, Z. Chen, A. Narita, K. Mullen, M. Bonn, M. Gensch, and D. Turchinovich, *Nature (London)* **561**, 507 (2018).
 [14] K. Kaneshima, Y. Shinohara, K. Takeuchi, N. Ishii, K. Imasaka, T. Kaji, S. Ashihara, K. L. Ishikawa, and J. Itatani, *Phys. Rev. Lett.* **120**, 243903 (2018).
 [15] N. Yoshikawa, K. Nagai, K. Uchida, Y. Takaguchi, S. Sasaki, Y. Miyata, and K. Tanaka, *Nat. Commun.* **10**, 3709 (2019).
 [16] B. Cheng, N. Kanda, T. N. Ikeda, T. Matsuda, P. Xia, T. Schumann, S. Stemmer, J. Itatani, N. P. Armitage, and R. Matsunaga, *Phys. Rev. Lett.* **124**, 117402 (2020).
 [17] C. P. Schmid, L. Weigl, P. Grössing, V. Junk, C. Gorini, S. Schlauderer, S. Ito, M. Meierhofer, N. Hofmann, D. Afanasiev, J. Crewse, K. A. Kokh, O. E. Tereshchenko, J. Gütde, F. Evers, J. Wilhelm, K. Richter, U. Höfer, and R. Huber, *Nature (London)* **593**, 385 (2021).
 [18] D. Golde, T. Meier, and S. W. Koch, *Phys. Rev. B* **77**, 075330 (2008).
 [19] G. Vampa, C. R. McDonald, G. Orlando, D. D. Klug, P. B. Corkum, and T. Brabec, *Phys. Rev. Lett.* **113**, 073901 (2014).
 [20] G. Vampa, C. R. McDonald, G. Orlando, P. B. Corkum, and T. Brabec, *Phys. Rev. B* **91**, 064302 (2015).
 [21] M. Wu, S. Ghimire, D. A. Reis, K. J. Schafer, and M. B. Gaarde, *Phys. Rev. A* **91**, 043839 (2015).
 [22] T. Otobe, *Phys. Rev. B* **94**, 235152 (2016).
 [23] T. Ikemachi, Y. Shinohara, T. Sato, J. Yumoto, M. Kuwata-Gonokami, and K. L. Ishikawa, *Phys. Rev. A* **95**, 043416 (2017).
 [24] N. Tancogne-Dejean, O. D. Mücke, F. X. Kärtner, and A. Rubio, *Nat. Commun.* **8**, 745 (2017).
 [25] T. T. Luu and H. J. Wörner, *Phys. Rev. B* **94**, 115164 (2016).
 [26] K. K. Hansen, T. Deffge, and D. Bauer, *Phys. Rev. A* **96**, 053418 (2017).

- [27] E. N. Osika, A. Chacón, L. Ortmann, N. Suárez, J. A. Pérez-Hernández, B. Szafran, M. F. Ciappina, F. Sols, A. S. Landsman, and M. Lewenstein, *Phys. Rev. X* **7**, 021017 (2017).
- [28] T. N. Ikeda, K. Chinzei, and H. Tsunetsugu, *Phys. Rev. A* **98**, 063426 (2018).
- [29] T. Tamaya, A. Ishikawa, T. Ogawa, and K. Tanaka, *Phys. Rev. Lett.* **116**, 016601 (2016).
- [30] I. Floss, C. Lemell, G. Wachter, V. Smejkal, S. A. Sato, X.-M. Tong, K. Yabana, and J. Burgdörfer, *Phys. Rev. A* **97**, 011401(R) (2018).
- [31] M. Lysne, Y. Murakami, M. Schüler, and P. Werner, *Phys. Rev. B* **102**, 081121(R) (2020).
- [32] A. Chacón, D. Kim, W. Zhu, S. P. Kelly, A. Dauphin, E. Pisanty, A. S. Maxwell, A. Picón, M. F. Ciappina, D. E. Kim, C. Ticknor, A. Saxena, and M. Lewenstein, *Phys. Rev. B* **102**, 134115 (2020).
- [33] J. Wilhelm, P. Grössing, A. Seith, J. Crewse, M. Nitsch, L. Weigl, C. Schmid, and F. Evers, *Phys. Rev. B* **103**, 125419 (2021).
- [34] H. Taya, M. Hongo, and T. N. Ikeda, *Phys. Rev. B* **104**, L140305 (2021).
- [35] G. Vampa, T. J. Hammond, N. Thiré, B. E. Schmidt, F. Légaré, C. R. McDonald, T. Brabec, D. D. Klug, and P. B. Corkum, *Phys. Rev. Lett.* **115**, 193603 (2015).
- [36] L. Li, P. Lan, L. He, W. Cao, Q. Zhang, and P. Lu, *Phys. Rev. Lett.* **124**, 157403 (2020).
- [37] T. T. Luu and H. J. Wörner, *Nat. Commun.* **9**, 916 (2018).
- [38] K. Uchida, V. Pareek, K. Nagai, K. M. Dani, and K. Tanaka, *Phys. Rev. B* **103**, L161406 (2021).
- [39] A. F. Kemper, B. Moritz, J. K. Freericks, and T. P. Devereaux, *New J. Phys.* **15**, 023003 (2013).
- [40] S. Y. Kruchinin, F. Krausz, and V. S. Yakovlev, *Rev. Mod. Phys.* **90**, 021002 (2018).
- [41] S. Ghimire and D. A. Reis, *Nat. Phys.* **15**, 10 (2019).
- [42] T.-Y. Du and C. Ma, *Phys. Rev. A* **105**, 053125 (2022).
- [43] R. E. F. Silva, I. V. Blinov, A. N. Rubtsov, O. Smirnova, and M. Ivanov, *Nat. Photonics* **12**, 266 (2018).
- [44] Y. Murakami, M. Eckstein, and P. Werner, *Phys. Rev. Lett.* **121**, 057405 (2018).
- [45] Y. Murakami and P. Werner, *Phys. Rev. B* **98**, 075102 (2018).
- [46] M. Lysne, Y. Murakami, and P. Werner, *Phys. Rev. B* **101**, 195139 (2020).
- [47] N. Tancogne-Dejean, M. A. Sentef, and A. Rubio, *Phys. Rev. Lett.* **121**, 097402 (2018).
- [48] S. Imai, A. Ono, and S. Ishihara, *Phys. Rev. Lett.* **124**, 157404 (2020).
- [49] K. Chinzei and T. N. Ikeda, *Phys. Rev. Res.* **2**, 013033 (2020).
- [50] C. Orthodoxou, A. Zaïr, and G. H. Booth, *npj Quantum Mater.* **6**, 76 (2021).
- [51] Y. Murakami, S. Takayoshi, A. Koga, and P. Werner, *Phys. Rev. B* **103**, 035110 (2021).
- [52] C. Shao, H. Lu, X. Zhang, C. Yu, T. Tohyama, and R. Lu, *Phys. Rev. Lett.* **128**, 047401 (2022).
- [53] T. Hansen, S. V. B. Jensen, and L. B. Madsen, *Phys. Rev. A* **105**, 053118 (2022).
- [54] J. Masur, D. I. Bondar, and G. McCaul, *Phys. Rev. A* **106**, 013110 (2022).
- [55] M. Udono, K. Sugimoto, T. Kaneko, and Y. Ohta, *Phys. Rev. B* **105**, L241108 (2022).
- [56] K. Uchida, G. Mattoni, S. Yonezawa, F. Nakamura, Y. Maeno, and K. Tanaka, *Phys. Rev. Lett.* **128**, 127401 (2022).
- [57] O. Grånäs *et al.*, [arXiv:2008.11115](https://arxiv.org/abs/2008.11115).
- [58] M. R. Bionta, E. Haddad, A. Leblanc, V. Gruson, P. Lassonde, H. Ibrahim, J. Chaillou, N. Émond, M. R. Otto, A. Jiménez-Galán, R. E. F. Silva, M. Ivanov, B. J. Siwick, M. Chaker, and F. Légaré, *Phys. Rev. Res.* **3**, 023250 (2021).
- [59] M. Imada, A. Fujimori, and Y. Tokura, *Rev. Mod. Phys.* **70**, 1039 (1998).
- [60] E. Dagotto, *Rev. Mod. Phys.* **66**, 763 (1994).
- [61] See Supplemental Material at <http://link.aps.org/supplemental/10.1103/PhysRevLett.129.157401> for the detail of the numerical methods, schematic figures and supplemental results, which includes Ref. [62].
- [62] P. Werner, H. U. R. Strand, S. Hoshino, Y. Murakami, and M. Eckstein, *Phys. Rev. B* **97**, 165119 (2018).
- [63] A. Georges, G. Kotliar, W. Krauth, and M. J. Rozenberg, *Rev. Mod. Phys.* **68**, 13 (1996).
- [64] M. Eckstein and P. Werner, *Phys. Rev. B* **82**, 115115 (2010).
- [65] H. Aoki, N. Tsuji, M. Eckstein, M. Kollar, T. Oka, and P. Werner, *Rev. Mod. Phys.* **86**, 779 (2014).
- [66] K. Sandholzer, Y. Murakami, F. Görg, J. Minguzzi, M. Messer, R. Desbuquois, M. Eckstein, P. Werner, and T. Esslinger, *Phys. Rev. Lett.* **123**, 193602 (2019).
- [67] M. Schüler, D. Golež, Y. Murakami, N. Bittner, A. Herrmann, H. U. Strand, P. Werner, and M. Eckstein, *Comput. Phys. Commun.* **257**, 107484 (2020).
- [68] P. Werner, H. U. R. Strand, S. Hoshino, and M. Eckstein, *Phys. Rev. B* **95**, 195405 (2017).
- [69] G. Martinez and P. Horsch, *Phys. Rev. B* **44**, 317 (1991).
- [70] G. Sangiovanni, A. Toschi, E. Koch, K. Held, M. Capone, C. Castellani, O. Gunnarsson, S.-K. Mo, J. W. Allen, H.-D. Kim, A. Sekiyama, A. Yamasaki, S. Suga, and P. Metcalf, *Phys. Rev. B* **73**, 205121 (2006).
- [71] Z. Lenarčič and P. Prelovšek, *Phys. Rev. Lett.* **111**, 016401 (2013).
- [72] D. Golež, J. Bonča, M. Mierzejewski, and L. Vidmar, *Phys. Rev. B* **89**, 165118 (2014).
- [73] M. Eckstein and P. Werner, *Sci. Rep.* **6**, 21235 (2016).
- [74] G. Vidal, *Phys. Rev. Lett.* **91**, 147902 (2003).
- [75] I. Kilen, M. Kolesik, J. Hader, J. V. Moloney, U. Huttner, M. K. Hagen, and S. W. Koch, *Phys. Rev. Lett.* **125**, 083901 (2020).
- [76] P. C. Becker, H. L. Fragnito, C. H. Brito Cruz, R. L. Fork, J. E. Cunningham, J. E. Henry, and C. V. Shank, *Phys. Rev. Lett.* **61**, 1647 (1988).
- [77] K. Nagai, K. Uchida, S. Kusaba, T. Endo, Y. Miyata, and K. Tanaka, [arXiv:2112.12951](https://arxiv.org/abs/2112.12951).
- [78] H. U. R. Strand, D. Golež, M. Eckstein, and P. Werner, *Phys. Rev. B* **96**, 165104 (2017).